Available online at www.sciencedirect.com
SCIENCE DIRECT®
Vision Research 44 (2004) 857–876
Vision Research
www.elsevier.com/locate/visres

# Intrinsic connections in tree shrew V1 imply a global to local mapping

David M. Alexander [a,f,*], Paul D. Bourke [b,f], Phil Sheridan [c], Otto Konstandatos [d], James J. Wright [e,f]

[a] Brain Dynamics Centre, Acacia House, Westmead Hospital, Hawkesbury Road, Westmead 2145, Sydney, Australia
[b] Centre for Astrophysics and Supercomputing, Swinburne University of Technology, 523 Burwood Road, Hawthorn 3122, Melbourne, Australia
[c] School of Computing and Information Technology, Griffith University, University Drive, Meadowbrook 4131, Brisbane, Australia
[d] School of Mathematics and Statistics, University of Sydney, City Road, Glebe 2006, Sydney, Australia
[e] The Liggins Institute, University of Auckland, 2-6 Park Avenue, Grafton 1001, Auckland, New Zealand
[f] Brain Dynamics Laboratory, Mental Health Research Institute of Victoria, 155 Oak Street, Parkville 3052, Melbourne, Australia

Received 19 December 2002; received in revised form 7 November 2003

**Abstract**

The local-global map hypothesis states that locally organized response properties—such as orientation preference—result from visuotopically organized local maps of non-retinotopic response properties. In the tree shrew, the lateral extent of horizontal patchy connections is as much as 80–100% of V1 and is consistent with the length summation property. We argue that neural signals can be transmitted across the entire extent of V1 and this allows the formation of maps at the local scale that are visuotopically organized. We describe mechanisms relevant to the formation of local maps and report modeling results showing the same patterns of horizontal connectivity, and relationships to orientation preference, seen *in vivo*. The structure of the connectivity that emerges in the simulations reveals a 'hub and spoke' organization. Singularities form the centers of local maps, and linear zones and saddle-points arise as smooth border transitions between maps. These findings are used to present the case for the local-global map hypothesis for tree shrew V1.
© 2003 Elsevier Ltd. All rights reserved.

*Keywords:* Primary visual cortex; Tree shrew; Neural networks; Orientation; Pinwheels; Neuroanatomy

## 1. Introduction

The identification of ocular dominance and orientation preference response properties in V1 led to the proposal of the *ice-cube* model to explain the organization of the response properties (Hubel & Wiesel, 1968, 1977). This model delineated a macrocolumnar unit of cortex, containing neurons responding preferentially to all possible orientations of visual stimuli at a particular position in visual space, delivered via both eyes. Further relationships between cytochrome oxidase (CO) blobs, orientation preference, ocular dominance, contrast, color and spatial frequency selectivity have since been identified (Blasdel, 1992; Blasdel & Salama, 1986; Horton & Hubel, 1981; Tootell, Switkes, Silverman, & Hamilton, 1988; Tootell, Silverman, Hamilton, Switkes, & De Valois, 1988; Tootell, Silverman, Hamilton, De Valois, & Switkes, 1988).

However, recent studies which produced coinciding maps of multiple response properties suggest there is not a rigid interlocking of response property systems in the manner described by the ice-cube model (Hubener, Shoham, Grinvald, & Bonhoeffer, 1997). Various authors have argued that the number and range of possible response properties, along with the need for local continuity in their mapping, precludes a crystal-like structure of the sort described by the ice-cube model. According to this view, the primary visual cortex achieves an approximately uniform coverage without a rigid interlocking of response property systems (Hubener et al., 1997; Swindale, Shoham, Grinvald, Bonhoeffer, & Hubener, 2000; cf. Basole, White, & Fitzpatrick, 2003).

A number of simulation-based models have been developed to account for the patterns of ocular

* Corresponding author. Address: Brain Dynamics Laboratory, Mental Health Research Institute of Victoria, 155 Oak Street, Parkville 3052, Melbourne, Australia.
*E-mail address:* dalex@mhri.edu.au (D.M. Alexander).

0042-6989/$ - see front matter © 2003 Elsevier Ltd. All rights reserved.
doi:10.1016/j.visres.2003.11.009

dominance, orientation preference and other response properties found in V1. In a review (Swindale, 1996), these models were classified into a number of categories, two of which are of particular relevance to this study.

The first category includes models depending upon neural network principles, originating from the work of von der Malsburg (e.g. Goodhill, 1993; Linsker, 1986; Miller, Keller, & Stryker, 1989; Obermayer, Ritter, & Schulten, 1990; Tanaka, 1989; von der Marlsburg, 1973). These models share a common set of postulates, namely the use of Hebbian synapses with normalized synaptic strength, spatio-temporal correlation in afferent activity during training, and connections between cortical neurons which are locally excitatory and inhibitory at slightly greater distance. Under these assumptions a realistic spatial ordering of response properties emerges in two-dimensional arrays of neurons.

Models in the second category provide an account of the same response organization in terms of dimension reduction (Durbin & Mitchison, 1990; Durbin & Willshaw, 1987; Kohonen, 1982; Mitchison & Durbin, 1986). Here the higher dimensional complexity of information in the afferents is reduced to the two-dimensional cortical surface. This dimension reduction is achieved by an inverse mapping endeavoring to satisfy two conflicting goals—namely, the need to maintain local smoothness of response properties within the cortical sheet, versus the need to ensure the sheet includes a compact, representative selection of features in stimulus space. Optimization of this mapping solution yields results very similar to the neural network models.

In a third type of model, Mitchison and Crick (1982) present an analysis of connectivity in the tree shrew based on a geometrical argument. Using simple rules, they derive some of the features seen when large amounts of tracer are injected into the supragranular layers of V1. The rules are: that regions with like orientation preference are connected to each other, and; that the strength of the connectivity drops off as a Gaussian function. The resultant connection geometry shows the stripe-like patterns seen to extend from the central injection site in the tree shrew (Rockland & Lund, 1982).

In this paper we outline an alternative (and complement) to the various models present in the literature, the local-global map (LGM) hypothesis. The LGM hypothesis has been reported briefly elsewhere (Alexander, Bourke, Sheridan, Konstandatos, & Wright, 1998). We suggest the response properties measured in V1 are a consequence of a basic organizational principle, the local map. This view is similar to Hubel and Wiesel's ice-cube model, without the requirement that response properties maintain rigid, repeating spatial relationships. The patterns of response properties are a function of the complex tiling patterns of the basic local map.

The most controversial aspect of the LGM hypothesis is that it proposes the existence of two, distinct, visuotopically organized mappings within V1. The first mapping is the standard, uncontroversial retinotopic mapping of the visual field to layer 4 of the primary visual cortex—the *global map* within LGM terminology. The second mapping is at the spatial scale of the orientation pinwheel (approximately 300 μm diameter) and tiles the surface of the primary visual cortex in the non-granular layers. This mapping—the *local map* within LGM terminology—supplies non-retinotopic response properties such as orientation preference. We argue that this local map, though modulatory in influence and not producing retinotopic response properties, is also visuotopically organized. [1] The germ of this idea was originally published in Schwartz (1980).

The next section reviews the relevant anatomical and functional features of tree shrew V1. In this paper we focus on the tree shrew, because in this animal the connectivity pattern described by the LGM hypothesis can be most easily established. Even so, our argument relies partly on the controversial idea that signals can travel horizontally via polysynaptic routes under specific stimulus conditions. To cover potential objections to this idea, in Section 3 we introduce concepts of neural synchrony. We show that synchrony can arise swiftly over distances larger than expected from purely anatomical considerations; the mechanism by which this occurs; and the implications for the development of visuotopically organized maps.

In Section 4 we describe two types of modeling to support our hypothesis. In the first we construct a geometrical argument similar to Mitchison and Crick (1982). We take as a starting assumption that the basic unit of connectivity is provided by the hypothesized local map. With this assumption, the stripe-like patterns seen upon injection of a large amount of tracer are reproduced. The second model is a neural network simulation of horizontal connectivity in the tree shrew, and the relationship of these connections to the orientation response. The purpose of this simulation is to provide *an illustration of the connectivity structure of the hypothesized local map*.

In the discussion we outline the implications of these various pieces of evidence in terms of the LGM hypothesis.

[1] In this paper we reserve the term 'visuotopically organized' to refer to the structure of a mapping at the most general level i.e. its topographic relationship to the visual field. A map may be said to be visuotopically organized, without reference to the response properties it supplies. The word 'retinotopic' will be used in a stricter sense to refer to mappings that are both visuotopic in structure and which supply the retinotopic response property i.e. locations within the map can be fired by stimuli at the corresponding position in the stimulus field.

## 2. Horizontal connectivity in V1 and its relationship to response properties

Layer 4 of V1 has a strict retinotopic organization (Blasdel & Fitzpatrick, 1984). In Layer 4 of the tree shrew the distortion of the visual hemi-field is much less marked than in other mammals (Bosking, Zhang, Schofield, & Fitzpatrick, 1997; Fitzpatrick, 1996), so that to a first approximation the retinotopic organization of tree shrew V1 may be regarded as the same shape as the visual hemi-field.

The geometry of orientation preference reveals three predominant features: singularities, linear zones and saddle-points (Blasdel, 1992). Orientation preference changes continuously around singularities, forming pinwheels. Between adjacent singularities are regions in which orientation preference changes slowly and continuously: called linear zones. Other regions between singularities show a local minimum in orientation preference in one direction and a local maximum in a perpendicular direction: called saddle-points. Singularities surrounding saddle-points form mirror images of each other, through orthogonal reflection lines.

Studies using injections of retrograde and antereograde tracer have revealed underlying regularities in patchy intrinsic connections within the supragranular layers of V1 (Blasdel, Lund, & Fitzpatrick, 1985; Bosking et al., 1997; Malach, Amir, Harel, & Grinvald, 1993; Rockland & Lund, 1983). These connections traverse the gray matter parallel to the cortical surface in the supragranular layers and project to discrete patches. Use of these tracer techniques, in conjunction with other imaging techniques, has revealed that patchy connections tend to prefer targets with the same response properties (Malach et al., 1993; Yoshioka, Blasdel, Levitt, & Lund, 1996). The spatial pattern of patchy intrinsic connections is therefore closely related to the spatial pattern of other response-property systems, such as orientation preference.

It has been shown, in tree shrew V1, that the patchy intrinsic connections are not perfectly radial, but form an elongated pattern (Bosking et al., 1997; Fitzpatrick, 1996). The axis of elongation corresponds to the preferred orientation of the injection site. In other words, if retrograde tracer is injected into a point in the supragranular layers with preferred orientation of $\theta$, the pattern of patchy intrinsic connections overlies a global, retinotopic representation of a line passing through that point and having an orientation $\Theta$ (where $\Theta$ of the line equals $\theta$ in the pinwheel of orientation preference).

In the tree shrew, unlike the monkey and the cat, these patchy intrinsic fibers may traverse the entire surface of V1 along the elongated axis. Along the longest V1 axis, running parallel to the vertical meridian, some fibers revealed by an injection site near the middle of this axis extend to over 80% of the total possible length (Bosking et al., 1997, Fig. 3B; Chisum, Mooser, & Fitzpatrick, 2003, Fig. 6A; Lyon, Jain, & Kaas, 1998, Fig. 4A). Connections along an axis aligned with the horizontal meridian traverse 100% of the extent of V1. Note that these figures are the maximum extent of the very long-range connections. Numerical analysis of these connections has revealed a logarithmic decrease bouton in density with distance from the site of injection (Chisum et al., 2003).

Though not generally acknowledged in visual neuroscience, the contribution of ipsilateral cortico-cortical connections cannot be ruled out. Such connections have been demonstrated in the kitten (Zuffery, Jin, Nakamura, Tettoni, & Innocenti, 1999, Fig. 3) and the macaque (Rockland & Knutson, 2001, Fig. 8). Such myelinated connections would provide rapid long-range dispersal of signal across V1.

An additional feature found in the tree shrew is that inputs from the non-classical receptive field are sufficient to fire a neuron in the upper layers (Fitzpatrick, 1996; cf. Lee, 2002). That is, a long bar which fires a neuron of appropriate orientation preference can also fire that neuron even when the region corresponding to the classical receptive field is blanked out from the stimulus. Under these circumstances, this neuron in the supragranular layers is not being fired by signals arriving directly from layer 4. The firing indicates that inputs arriving from horizontal connections via polysynaptic routes can exert a powerful influence.

Consistent with this polysynaptic influence, many layer 2/3 neurons in tree shrew V1 exhibit length summation—increasing firing rates to increasingly long stimulus lines (Chisum et al., 2003). Length summation occurs in some neurons for stimuli up to 40° of visual angle (Bosking & Fitzpatrick, 1995): almost the entire extent of the visual field represented in tree shrew V1. When the length summation response is averaged over all neurons measured in layers 2/3 (i.e. regardless of length preference), the response curve still trends slightly upwards at the maximal extent of stimuli tested (Chisum et al., 2003). Further length summation experiments, using lines extending to 50° of visual angle (~100% of V1 representation), will help establish the maximum length preference.

When large injections of tracer are made into the surface of tree shrew V1 (Rockland & Lund, 1982), a widespread pattern of connections results. The prominent feature is a series of stripe-like regions that extend from the injection site, interdigitated with rows of no tracer uptake. Occasional cross-stripes run for short distances in a perpendicular direction. A third feature is elongated patches at the furthest extent of tracer uptake. Consistent with observations from focal injections, large injections of tracer reveal connections that traverse virtually the entire extent of V1 (Rockland & Lund, 1982, Fig. 1B).

In the modeling of horizontal connectivity in the tree shrew, presented in Section 4, the long-range patchy fibers are assumed to be a major source of orientation tuning. Orientation response is weak in the layer 4 of the tree shrew, and the anisotropic horizontal connections seen in macaque layer 4 are largely lacking (Fitzpatrick, 1996). The projections from layer 4 to the supragranular layers are radial and isotropic (Chisum et al., 2003).

In our neural network simulations, we assume an initial set of widespread but weak connections, from which the long-range patchy connections develop. Little is known about the development of these connections in the tree shrew. According to Ungersbock, Kretz, and Rager (1991), the synaptic density in layer 3 of the tree shrew climbs linearly from birth till day 30, when it begins to plateau. Suturing experiments in the tree shrew suggest that diffuse non-patchy connectivity is present early in development, showing the same spread as the patchy connectivity seen in mature animals (Crowley, Bosking, Foster, & Fitzpatrick, 1996). Consistent with this, anatomical studies of development of area 17 in the Ferret suggest the patchy intrinsic connections are winnowed from an initially diffuse set of non-patchy connections in the upper layers (Ruthazer & Stryker, 1996). Together, these observations appear consistent with our assumption initially diffuse but widespread connections. The spatial extent of initial diffuse connectivity in the tree shrew has not been firmly established, however, due to methodological uncertainties (David Fitzpatrick, personal communication).

The anterograde tracer techniques used in tree shrew V1 show axonal targets of neurons spreading *from* a site of tracer injection (Bosking et al., 1997). However, since like orientation preference connects to like, the connections are *reciprocal*, and axonal targets *to* a similar site would look much the same. Inputs located along a global line $\Theta$ converge into the orientation pinwheel at orientation preference $\theta$. The pattern of inputs into a pinwheel, therefore, recapitulates the global map in the $\Theta$ dimension. The primary difference between the two mappings is a doubling of the visuotopic angles in the pinwheel, so the two halves of the globally represented line project to the same place in the pinwheel. This idea, that the response properties at a local scale arise from a remapping of V1's global retinotopic map, is central to this paper.

A specific prediction of the LGM hypothesis is that horizontal connections originating from singularities will be much shorter than horizontal connections originating beyond the vicinity of singularities. This prediction has recently been confirmed in both the cat (Yousef, Toth, Rausch, Eysel, & Kisvarday, 2001) and the ferret (Lund, Angelucci, & Bressloff, 2003). The reasoning behind this prediction is given in Section 4 and the discussion.

## 3. The importance of synchronous neural activity

In this section we establish three arguments. The first deals with evidence that neural synchrony can be established swiftly over distances within V1 that are much greater than expected based on purely anatomical considerations. The second argument describes how synchrony is established between sites that are not within 1 mm of each other i.e. do not have dense interconnections; this has consequences for visual development and the assumptions behind the neural network simulations. The third argument assesses the role of neural synchrony in the development of visuotopic maps, both at the global scale of V1 and at a more local scale. To our knowledge, no data on synchronous neural activity are published for the tree shrew (Medline search for "tree shrew" and "synchrony" produces no results). This section therefore relies on findings from other mammals; as well as simulation results regarding neural synchrony from our group (for an overview see Wright et al., 2001).

### 3.1. Horizontal diffusion of signal within V1

The assumption that inputs from the visual field to V1 result in wide dissemination of information throughout V1 seems counter-intuitive to many anatomists and physiologists. Conventional expectation is that inputs to V1 are constrained by the strong inhibitory nature of surround effects, precluding propagation of signals through a cascade of lateral connections (Angelucci et al., 2002). Even where very long range connections exist, the density of connections beyond the minimum discharge field is not considered sufficient to substantially effect response tuning (Chisum et al., 2003). The orientation preference response is assumed, therefore, to be limited stimulus features of small separation in the visual field. This restricted interpretation may not be correct, for reasons involving the mechanism of synchronous oscillations.

Measurements of synchronous oscillation in vivo show that while neurons interact powerfully at a local scale, they also interact over larger distances. Zero phase-lag synchrony is found in the gamma-band over distances within V1 as large as 5 mm in the monkey (Frien & Eckhorn, 2000; Livingstone, 1996) and 7 mm in the cat (Gray, Konig, Engel, & Singer, 1989). More recent findings, which assume gamma synchrony is the result of propagating wave activity, reveal wave interactions with a modal half-height at 9.5 mm distance in the monkey (Eckhorn et al., 2001) and 5 mm in the rabbit—with some cases extending up to 2 cm (Freeman & Barrie, 2000).

Another objection raised against the occurrence of widespread horizontal interactions within V1 concerns the speed at which signal can propagate i.e. polysynaptic

routes are too slow for visual processing (Angelucci & Bullier, in press). Estimates using optical imaging techniques in the monkey indicate that signal propagates horizontally within V1 at speeds of 0.1–0.2 m/s (Grinvald, Lieke, Frostig, & Hildesheim, 1994; Slovin, Arieli, Hildesheim, & Grinvald, 2002). Measurements in the cat visual cortex, using electrophysiological techniques, are consistent with this, although some speeds were recorded of up to 1.0 m/s (Bringuier, Chavane, Glaeser, & Frégnac, 1999).

However, theoretical results indicate that cortical wave-activity does not obey simple, non-dispersive laws (Rennie, Wright, & Robinson, 2000). Instead, the velocity of propagation is a function of frequency. Measurements that account for frequency of the signal provide estimates of speed of propagation that increase with frequency. Analysis of gamma-band activity in the monkey visual cortex indicates propagation speeds of 0.1–1.0 m/s, with a modal speed of 0.4 m/s (Reinhard Eckhorn, personal communication) and similar results are found for the rabbit (Freeman & Barrie, 2000). At 60–80 Hz. almost half of the 'phase-cones' in rabbit V1 propagate at speeds $\geqslant 2.0$ m/s.

### 3.2. Connectivity and synchronous oscillation

The results regarding synchronous oscillation present quite a different picture to that derived purely from circuit-based anatomical considerations. Dense regions of horizontal patchy connectivity, in the monkey, project to no more than 1 mm distant from the site of injection. Yet zero-lag synchronous oscillation can be measured, between sites of the same orientation preference, up to 5 mm distance in monkey V1. Our previous simulation results suggest that synchrony between these distant sites is bound together by an associativity rule (Wright, Bourke, & Chapman, 2000).

(a) Synchrony can be established between any two concurrently stimulated sites, (A,B), provide they have sufficiently strong mutual connections between them. The synchrony is established with a latency almost equal to the speed of axonal conduction between the sites.
(b) Likewise B can establish synchrony with C, if B is mutually connected to C and both sites are concurrently stimulated. If A is not directly connected with C, however, A cannot enter synchrony with C by direct axonal connection.
(c) However A, B and C can form a synchronous chain, mediated from A to C via B, if all receive concurrent inputs from the visual field. Transmission of information will occur $A \leftrightarrow C$, and onset of synchrony can occur almost as fast as axonal propagation delays over this distance (Chapman, Bourke, & Wright, 2002).

On this view, synchrony acts as a 'virtual' connectivity mechanism, with the gamma-band carrier signal opening up a window of information transmission. Thus information from a single extended stimulus in the visual field is relayed to all activated points in V1, as if a one to all connectivity was present.

This mechanism establishes synchrony only under the appropriate stimulus conditions. Our previous simulation results indicate that each of the points A, B and C must be concurrently stimulated (Wright et al., 2000). In the tree shrew, these points correspond to the local maxima in activity seen with optical imaging when a single bar is presented as a stimulus (e.g. Bosking, Crowley, & Fitzpatrick, 2002, Fig. 1). These local maxima coincide with patches of a particular orientation preference (equal to the angle of the bar stimulus). Under these specific conditions, signal arising from local maxima along the entire representation of a long bar (40°+) can contribute non-trivially to synchronous oscillation measurable at any other such local maxima.

The speed at which synchrony is established may seem counter-intuitive to many visual anatomists. Our modeling indicates that when A, B and C are concurrently stimulated, signal components common to the activity at A, B and C are preferentially amplified, while signal components not held in common are attenuated. Measurements in vivo likewise indicate that synchrony onset between distant sites is too fast to be accounted for simply by the arrival and retransmission of a common driving signal (Gray, Engel, Konig, & Singer, 1992).

Chisum et al. (2003) argue that patchy connections will have most influence within the minimum discharge field i.e. within 1 mm. This begs the question, however, as to the role of the relatively rare, very long-range connections seen in the tree shrew. Freeman and Barrie (2000) have suggested that this class of connections, though weak in influence, nevertheless play an important role. The proposed role relies on the exquisite dynamical sensitivity of the cortex. A relatively small number of synaptic contacts, under appropriate dynamical conditions, are sufficient to flip cortical attractor dynamics from one basin to another (Freeman & Barrie, 2000). Any very long-range connections $A \leftrightarrow C$, despite their rarity, enhance the rapid transition to a synchronous chain $A \leftrightarrow B \leftrightarrow C$.

This mechanism proposed in *a–c* above has consequences for the development of very long-range horizontal connections. The mechanism would allow these connections to reach appropriate targets, even in the absence of diffuse, very long-range connectivity in the immature animal. Episodes of axonal outgrowth and synaptogenesis during development (Ungersbock et al., 1991) serve to provide fibers of appropriate length. Since A is readily able to establish synchrony with C in the absence of monosynaptic connections, Hebbian mechanisms can provide the necessary fine-grained guidance

so that like-connects-to-like connections can be established. For reasons of computational efficiency, however, the neural network simulations described in Section 4 assume an initial diffuse, all to all connectivity in the upper layers. Dynamical simulations, of resolution sufficient to demonstrate the connectivity patterns of interest here, are several orders of magnitude beyond current computational capabilities.

### 3.3. Development of visuotopicaly organized maps

Zero-lag synchrony provides an essential component of Hebbian synaptic modification—i.e., activity at pre- and post-synaptic neurons is concurrent for interacting neurons in extended neural ensembles. This correlated activity enables sets of reciprocal connections to store information about stimulus objects. This consideration, coupled with consideration of average densities of synaptic connectivity in the cortex, and the statistical properties of stimuli in the visual field, has implications for the way orientation maps in V1 could arise:

Let $\Delta P$ be distances in the visual stimulus ($S$) field, $\Delta p$ distances of separation on the V1 cortical surface, or field, $r(\Delta p)$ the average zero-lag correlations at separation $\Delta p$ in the V1 field, and $R(\Delta P)$ the average spatial autocorrelation at separation $\Delta P$, of stimuli in $S$. We can then note:

(1) In general the strength of connectivity between cortical neurons declines with distance of separation (Braitenberg & Schuz, 1991), and decreased connectivity lowers the magnitude of average zero-lag synchrony between the neurons. That is, $r(\Delta p) \propto (\Delta p)^{-1}$.
(2) Natural stimuli in the visual, or other sensory field, have spatial autocorrelations generally decreasing with distance of separation, simply because closer points in an image blur into identity. That is, $R(\Delta P) \propto (\Delta P)^{-1}$. Randomly presented input also has this general property, so long as the inputs have decreasing autocorrelation with increasing spatial separation—i.e. that they are spatially "brown" noise.
(3) Mexican-hat surround inhibition creates conditions whereby activity at one locus tends to suppress activity at others, and combined with Hebbian learning, synapses then compete with each other to increase their relative coupling strength. In this competition, more strongly coupled neurons have an advantage in retaining their mapping of autocorrelations in the stimulus field.

These considerations ensure that stable synaptic mappings, $S \rightarrow V1$ are such that, generally, $R(\Delta P) \rightarrow r(\Delta p)$. *This means that the strongest-coupling relations, (and therefore generally the nearest-neighbor connections) in the cortex will store information concerning the largest spatial autocorrelations in the visual field.* This pattern of storage does not always amount to a simple 1:1, nearest-neighbor to nearest-neighbor, mapping of visual field to visual cortex. Whatever the complexities of the mapping, the relationship of spatial autocorrelation to average zero-lag synchrony requires a systematic relationship between the two fields.

Synaptic coupling maps can obey these storage constraints in two complementary ways.

(a) Nearest-neighbor relationships will be partially retained between stimulus configurations and the global mapping into layer 4 of V1. Locality in the visual field is mapped in a retinotopic fashion to locality in the cortical field.
(b) The emergent connectivity of the cortical surface may take the form of a tiling by many local maps, each of which conforms to the mapping $R(\Delta P) \rightarrow r(\Delta p)$

The second possibility, (b), contrasts with the first, (a), in several important ways.

(1) Such maps are likely to arise when contextual information is being learned, i.e. conditional on activity at point $P$ in the global map, what is the set relationships between spatial autocorrelations in the visual field?
(2) Secondary associations between homologous areas within each of the local maps arise as connections between maps, as a subset of the mapping $R(\Delta P) \rightarrow r(\Delta p)$. These are the horizontal patchy connections that connect like regions of orientation preference to like and allow horizontal transmission of signal between these sites.
(3) Each local map is subject to the same kind of topographical consistencies as is the global map. Therefore each part of each local map must vary systematically in its relationship to the visual field.
(4) The storage of spatial autocorrelations has the further effect of eliminating redundant features in the stimulus configuration. One example of redundancy elimination is the representation of $2\pi$ of visual space in $\pi$ of orientation preference (see end of Section 2)—synaptic storage of this type could not discriminate between lines oriented at 0 and $\pi$ of rotation.
(5) The storage of spatial autocorrelations will add redundancies where features are common to several stimulus types. An example of redundancy addition is the re-representation of local space (i.e. point $P$ in (1) above) regardless of the shape of the object. In the case of representing both short and long lines of various angles, all of which pass through point $P$, then point $P$ will be re-represented throughout the local map.

Our argument, in essence, is that the organization of the stimulus field, in conjunction with mechanisms involving neural synchrony, is likely to lead to visuotopically organized maps. These maps can be retinotopic (i.e. the global V1 map) or maps of non-retinotopic response properties. If widespread signal propagation is allowed, there is no in-principle reason why additional visuotopically organized maps would not arise at a more local scale of V1.

Despite the lack of data on synchronous oscillation in the tree shrew, there are two factors (described earlier) which suggest the conclusions drawn from this section are likely to apply at least as strongly to the tree shrew: First, the spread of horizontal connections is 80–100% of the extent of the global map; and second, inputs from outside the classical receptive field, alone, are sufficient to drive some neurons in the upper layers. Together these two factors suggest that, under the appropriate stimulus conditions and aided by the mechanism of neural synchrony, signal is able to propagate horizontally across the entire extent of V1 in the tree shrew. This conclusion is supported by the observation that some neurons in the upper layers display length summation for bars at least as large as 40° of visual angle.

## 4. Modeling of long range horizontal connections

### 4.1. A geometric model

In the geometric model we assume that horizontal connectivity patterns in the supragranular layers of the tree shrew have a characteristic form: singularities receive input from short-range fibres (Lund et al., 2003; Yousef et al., 2001) and orientation patches receive input from long range-fibers (Bosking et al., 1997; Fitzpatrick, 1996). We also assume that connectivity in the primary visual cortex in mammals is organized into columnar modules, as described by Lund et al. (2003). The short-range horizontal connections to the singularity are organized into a central column, and regions of widespread connectivity are organized into other discrete columns like spokes around this central hub.

Since each dendritic tree can potentially sample from several of these columns, neurons with smoothly varying receptive field properties result (Edwards, Purpura, & Kaplan, 1995). For example, a neuron situated on the border of the central column would receive inputs from both the short-range fibers and inputs from a column with widespread connectivity, resulting in a preference for medium length bars. This discrete view of *horizontal connectivity organization* is therefore consistent with a continuous, smoothly changing mapping of *response properties* such as orientation preference.

Other features of the orientation preference map, such as linear zones and saddle points, can be explained as tiling patterns of the 'hub and spokes' local connectivity map. The relationship between singularities, saddle-points and linear zones, as a function of tiling pattern, is illustrated in an idealized form in Fig. 1a. The basic pattern of tiling is one in which adjacent local maps are reflected about tile borders. This tiling pattern creates a saddle-point at the meeting point of four adjacent tiles. If one row from this tiling pattern is shifted left or right by one tile space, a pattern of vertically arranged of linear zones results. In the geometric modeling we use a discrete representation of the local map (Fig. 1b) since we are concerned with the underlying connectivity map rather than the orientation map *per se*.

The connectivity data provided by Bosking et al. (1997) result from highly focal injections into a single patch of uniform orientation preference. The Rockland and Lund (1982) data provide a test of our hypothesis at a slightly larger scale because tracer was injected into a large region of the surface of V1. This region is therefore likely to encompass at least one pinwheel of orientation preference. The connectivity revealed by such injections shows patterns not seen in the focal injection data (though intimately related). We were therefore interested in whether this pattern from large tracer injections

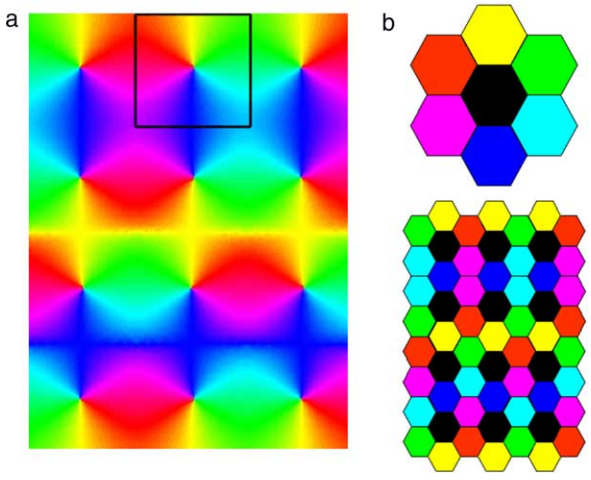


Fig. 1. (a) Idealized illustration of tiling pattern of orientation preference maps. The basic map of orientation preference, with a singularity at the center, is shown with the black border. There are two tiling patterns that allow orientation preference to change smoothly across map borders: 1. The upper part of the figure shows adjacent singularities that are reflections of each other. This creates the saddle-point pattern. 2. The third row of orientation preference maps has been shifted across by one column. This creates a series of linear zones, running vertically, in the lower half of the figure. (b) Idealized illustration of the hypothesized columnar organization of connectivity (see text for details). The upper figure is the discrete equivalent of the local map shown in the square in the left portion of the figure. The lower figure is the discrete version of the entire continuous mapping to the left. While the orientation preference map is assumed to be continuous in nature (seen main text, Section 4) we provide the discrete map for comparison because it describes the purported underlying columnar structure of the connectivity, and it is used in the geometric argument in Section 4.

can be reproduced *when the starting assumption is that the primary unit of connectivity is a hub and spokes local map centered on the singularity*.

We used a rule-based model, similar to Mitchison and Crick (1982):

1. The maps of orientation preference are formed from a tiling of the hypothesized primary unit of connectivity.
2. Discrete columns connect to other discrete columns of the same type, provided.
3. They are contained within the shape of a globally represented bar, of appropriate orientation (the spokes). Since each column of connectivity in the model covers 30° of orientation, all possible bars within this 30° range are included within the global shape. This results in a 'bow-tie' pattern of tracer uptake for each individual column type (see the individual maps in Fig. 2a). For example, columns with orientation preference of −15° to 15° connect to other columns with this same orientation preference provided they both fall within the bounds of the set of globally represented oriented bars, −15° to 15°, centered within the injection site.
4. In the case of the central column containing the singularity, the corresponding global object is blob shaped, resulting in shorter-range isotropic connections (the hub).

The assembled connectivity map, with both saddle-point and linear zone tilings, is shown in Fig. 2b. The maps of connectivity resulting from this geometrical argument are qualitatively similar to those in the Rockland and Lund (1982) data. The chief feature is the stripe-like pattern that emerges from the central injection site, particularly prominent in the linear zone region of the image (lower half). However, other features are present which are not seen in the Mitchison and Crick (1982) model. In particular, the occasional 'cross-stripe' seen in the Rockland and Lund (1982) data is a prominent feature in the saddle-point region of the image (upper half). The elongated patches seen at the extremities of tracer uptake are also present in both the saddle-point and linear zone examples. Variants of this model, e.g. including larger regions in the 'injection' zone, or rotating the local map, did not make any qualitative difference to the results.

A number of testable predictions arise from this geometric model. First, singularities will tend to appear in the inter-stripe regions of the stripe-like pattern, due to their shorter-range connections (see Fig. 2b). Without a central hub in the connectivity maps, singularities fall on the borders of stripe/inter-stripe regions (data not shown). Second, the stripe-like pattern will be associated with the linear zone tiling and the cross-stripe pattern will be associated with saddle-point tiling. While this second prediction does not depend on the presence of a central hub, it is a consequence of the idea that saddle-points and linear zones result from tilings of the basic local map.

An important observation can also be made about the spatial frequency of features in the orientation preference map. As can be seen in Fig. 2a, the spatial frequency of columns of a particular orientation preference (e.g. −15° to 15°) can vary depending on the exact tiling pattern (i.e. saddle-point or linear zone), and the overall rotation of local map. Despite the rigid tiling of the underlying map in this simple geometric model, the spatial frequencies of the orientation columns vary. Likewise, the variegated connectivity map shown in Fig. 2b does not at first glance reveal an obvious relationship to the rigid tiling of local maps. In the neural network simulations to follow, we will show that the hub and spokes local map connectivity arises under conditions where the overall map of orientation preference is much more noisy; that is, where the tiling patterns are more variable.

### 4.2. Assumptions behind the neural network simulations

The neural network simulations of V1 focus on horizontal intrinsic connectivity, its role in orientation preference, and aims to explain data from the tree shrew. The details of the neural network simulation are described in Appendix A. Assumptions in the simulations of horizontal connectivity in the tree shrew include:

(a) Cortical elements within a local neighborhood interact via a standard excitatory-center/inhibitory-surround (a so-called *Mexican-hat field*).
(b) The retina projects to the primary visual cortex in the standard retinotopic manner, but additional to this *direct* retinotopic mapping, any point in the supragranular layers may contribute some input to any other point. These *indirect* projections are initially weak and diffuse and are modulatory in influence i.e. do not contribute to the retinotopic response property.
(c) Hebbian learning applies to excitatory synapses supplying cortical input to the supragranular layers via the indirect, diffuse pathway (Constantine-Paton, Cline, & Debski, 1990; Friedlander, Fregnac, & Burke, 1993; Rauschecker, 1990). For reasons of computational efficiency, Hebbian learning was not applied to the Mexican-hat fields, nor the direct inputs.

These simulations therefore belong to the first category of model described in the introduction—that of neural networks, differing in emphasis from earlier models in only one respect of relevance. The further assumption of (b) is made that any point in the input

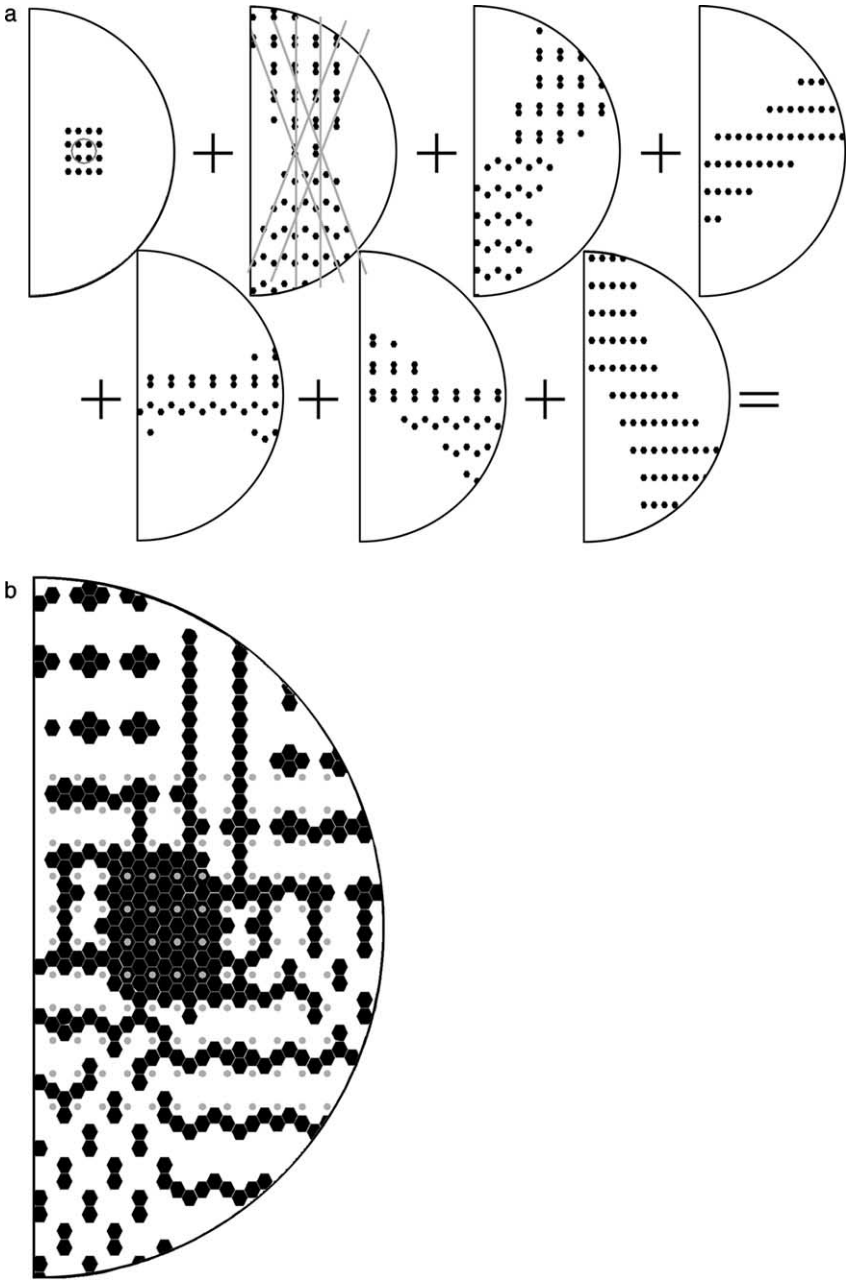


Fig. 2. (a) The component images from which the geometric model is constructed. These images demonstrate the rules on which the geometric model is based. The first component image shows the pattern of short-range horizontal connections emerging from the central columns (hub) of each local map (marked black in Fig. 1b). This image also shows the extent of tracer injection (grey circle). In the other six component images, columns of a particular orientation preference connect to like columns, provided they both fall within the shape of a bar of that orientation (spokes). Since each column covers a range of orientations, and the injection site covers several local maps, the resulting component images are 'bow-tie' in shape. The second image shows a subset of the global lines that fall within this bow-tie shape (grey lines). These component images also demonstrate that iso-orientation patches repeat at a different spatial frequencies, despite the use of a rigid tiling pattern of local maps. The spatial frequency depends upon the type of tiling involved (saddle-point in upper half of each image and linear zone in bottom half) and the rotation of the local map. See Fig. 1 and beginning of Section 4 for a description of the relationship between the orientation preference maps, and the underlying connectivity columns. (b) Connectivity patterns resulting from the geometric model. The diagram shows the modeling of the effects of a large injection of tracer into the surface of V1. The upper half of the model V1 was made using a saddle-point tiling pattern, and the bottom half made using the linear zone tiling pattern (see Fig. 1b). The rules governing the model are explained in the main text. The connectivity pattern results from combining the component images shown in (a). The resultant connectivity pattern shows the primary feature of stripe-like regions extending horizontally from the central zone of injection. Another feature present is cross-stripes seen in the saddle-point region (upper half of image) that run vertically. Note also the elongated patches seen at the extremities (prominent in the top left and bottom left). Each of these features is present in the in vivo connectivity (Rockland & Lund, 1982). The positions of the central band of singularities is shown with grey dots. Outside the injection zone, the singularities are seen to fall within interstripe regions.

field can potentially influence any point in the supragranular layers. While it is unclear whether diffuse, direct connections exist at the appropriate scale in the immature tree shrew (see Section 2), we have argued that, in the absence of widespread immature connections, mechanisms involving synchronous oscillation can play an equivalent role (see Section 3). For computational convenience the present neural network simulations begin with all-to-all random, weak connectivity. The present model is a static, time-averaged portrayal of what is never the less a *dynamical* wave-medium. While more realistic dynamics (Chapman et al., 2002; Robinson, Wright, & Rennie, 1998; Wright, 1997; Wright et al., 2000) will add to the explanatory scope of the modeling, the present description attempts to capture the essential *structural* mechanisms involved in the development of horizontal connectivity.

The basic unit of the neural network simulation is at the scale of the minicolumn (30 μm). This choice allows simulation of networks at the scale of V1. It is assumed that minicolumns, as aggregates of neurons, behave in a similar fashion to individual neurons for the purposes of studying network self-organization.

A moving bar was repeatedly swept across a simplified model retina. Activity in this retina then drove activity in the model granular layer, which in turn activated the model supragranular layer, via *direct* and *indirect* pathways. The direct pathway simply projects the retinotopic map of the granular layer into the supragranular layer. The indirect pathway is the initially all-to-all, weak and diffuse connectivity in the supragranular layer. The direct and indirect pathways are illustrated in Fig. 3. Two configurations of indirect connectivity are shown. Both achieve the required diffusion of information throughout the cortex, from the input retinotopic map. The appropriate type of indirect connectivity was applied within different simulations to enable computation over cortical areas of sufficient resolution (see Appendix A). The effects of local supragranular interactions were then added, using a simplified excitatory-center and inhibitory-surround mechanism.

In these simulations we use a learning rule derived from the coherent infomax principle (Phillips & Singer, 1998; see Appendix A). Though related closely to Hebbian learning, this learning rule differs in some critical aspects. It can be succinctly described as a ''floating hook'' function, where the main diagonal of the hook connects together units that fire in correlated fashion (and disconnects units whose firing patterns are negatively correlated) according to Hebbian principles. The 'floating' aspect of the rule enables neurons to be sensitive to the context of their own history of firing, adjusting the balance point of learning vs. unlearning to maximize contextually relevant information (Phillips & Singer, 1998). That is, under-utilized units in the simulation strengthen their connections quickly to any pattern of positively correlated activity in which they become engaged; units with an average firing rate above the desired level have connections quickly weakened by any negatively correlated patterns of firing. Combined with the soft 'winner-take-all' conditions imposed by the excitatory-center/inhibitory-surround mechanism, this aspect of the learning rule forces each local neighborhood of units to gain a representation of a wide range of contexts. These contexts are stored as varying patterns of modulatory connections into the different units within the local neighborhood.

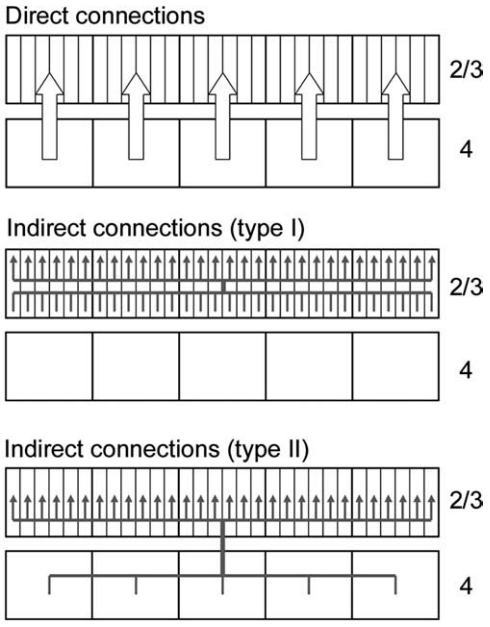


Fig. 3. Input connections used in the two versions of the neural network simulations. The upper figure shows direct connections (large arrows), which supply input from each retinotopic position in the layer 4 (rectangles, thick lines) to each retinotopic position the layers 2/3 (rectangles, thick lines). The middle figure shows indirect (type I) connectivity (gray arrows). Each minicolumn in the supragranular layer (rectangles, thin lines) is connected to every minicolumn in the supragranular layer. The lower figure shows indirect (type II) connectivity (grey arrows). Each retinotopic position in the granular layer is connected to every minicolumn in the supragranular layer.

We show that with the assumptions outlined in the preceding paragraphs, the network self-organizes so that short, blob-like stimuli are represented in and around the singularities, and long, bar stimuli are represented away from the singularities. This finding supports our assumption of a hub and spokes local connectivity map. The other notable features of the map of orientation preference, saddle-points and linear zones, emerge as smooth transitions between tilings of this basic local map, as also assumed in the geometric model.

### 4.3. Neural network simulation results

The presentation of a line to the model retina is shown in Fig. 4c. An example of the model supragranular

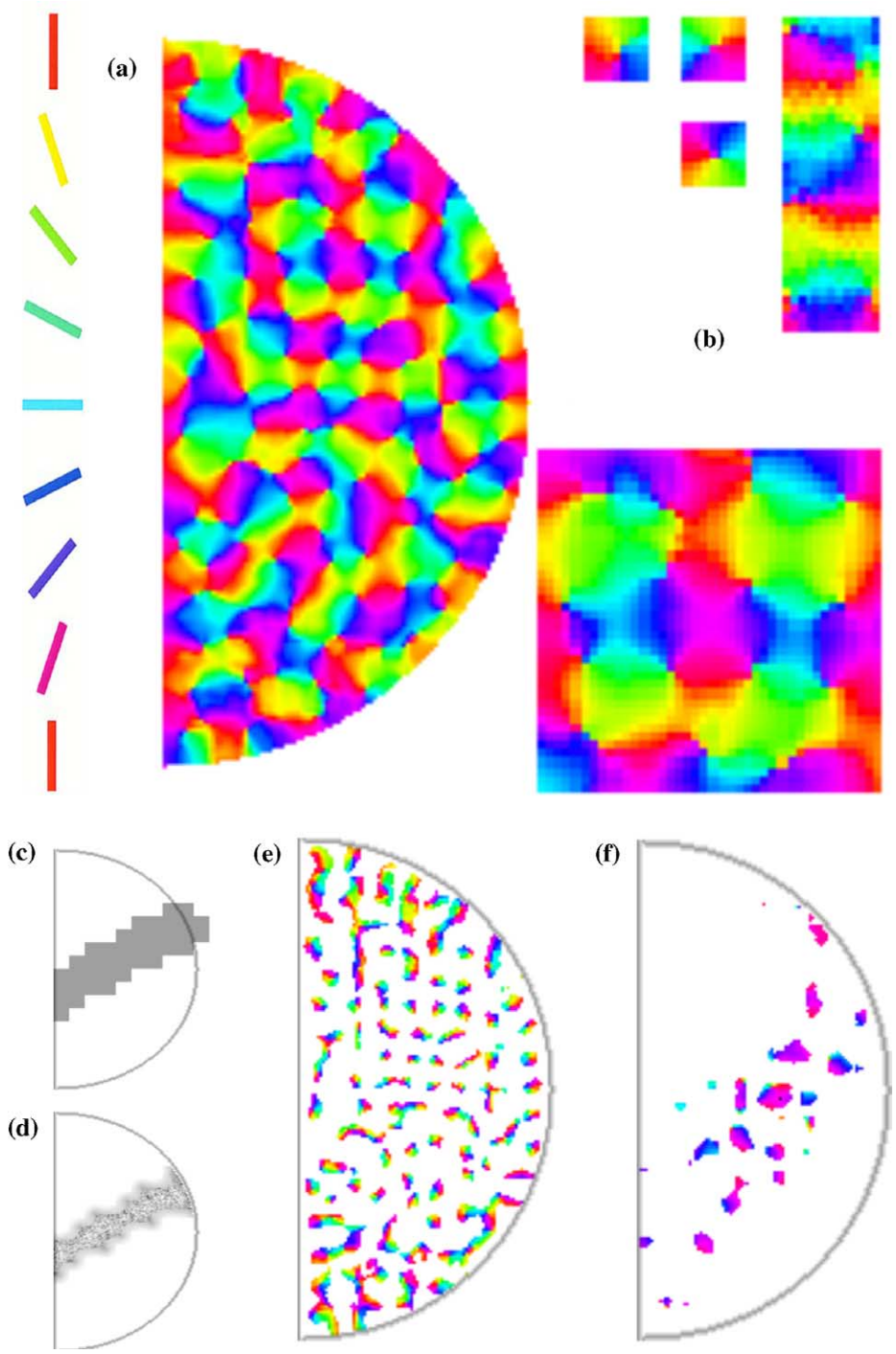


Fig. 4. Simulation of orientation preference in the LGM model using type I indirect connectivity. In this experiment the network was stimulated with moving bars only. (a) Map of orientation preference. The map is produced in a manner analogous to the orientation preference maps in vivo (see Appendix A). (b) Detail shows singularities, linear zones and saddle-points (three small squares, long strip and large square, respectively). The preponderance of near vertical orientation preferences on the straight edge of the semi-circle is an artefact of the boundary of the simulated cortex. (c) Retinal image of line projected onto granular layer. (d) Raw image of cortical activity in the supragranular layer. Grey levels show the activation level due to the direct and indirect inputs, as modified by the excitatory-center/inhibitory-surround mechanism. The activation varies from 0 (white) to 1.5 (black). This image is taken from early in network evolution. (e) Regions in which the orientation selectivity was low also show highest rate of change in orientation preference. (f) Simulated horizontal patchy connectivity and relationships to orientation preference. Patterns of connectivity from a single minicolumn in the middle of an iso-orientation patch in the supragranular layers (site of simulated tracer injection shown with black dot). The sites where the connections terminate are colored with the orientation preference at those points in the map. The connections traverse the entire surface of V1, connect to regions of similar orientation preference as the site of origin, and overlie the shape of an oriented line having of an angle matching the orientation preference of the site of tracer injection. The local halo of non-patchy connectivity is not seen as these connections were not modeled explicitly as connections (see text).

layers, activated by a bar, is shown in Fig. 4d. This image is taken from early in the developmental sequence, hence the 'salt and pepper' appearance of the activations. A map of orientation preference in the model tree shrew V1 is shown in Fig. 4a. The simulation was run for 20,000 time-steps (400 sweeps of the stimulus bar).

The simulated orientation preference map shows singularities, saddle-points and linear zones and has the same qualitative flavor as orientation preference maps from the tree shrew, macaque, cat or ferret primary visual cortex. Fig. 4e shows the corresponding map of the low magnitude regions, with orientation preferences superimposed. This simulation result also reflects animal data: lower magnitude regions coincide with high rates of change of orientation preference (Blasdel, 1992). The figure shows only singularities and fractures as having a low magnitude vector sum.

Fig. 4f shows the connection pattern of the model intrinsic connections in the supragranular layers. The projections (using the simulation equivalent of 'anterograde tracer') terminate in patchy regions that have the same orientation preference as the site of injection. In addition, the pattern of patchy connections is elongated so that it coincides with the retinotopic projection of a line of that orientation. The connection patterns found using simulation 'retrograde' and 'antereograde' tracer were essentially identical, both obeying the like-connects-to-like principle seen in animal studies.

One set of connections seen in the tree shrew is missing from this diagram—the local halo of non-patchy connectivity that is the presumed origin of the excitatory-center and inhibitory-surround mechanism (Swindale, 1996). These connections are not explicitly modeled in the simulations *as connections* (see Appendix A). The algorithm used to model these connections nevertheless introduces an additional set activations that tend to be inhibitory in effect within the 'rim' of the Mexican-hat. The coherent infomax learning rule used in the simulation does not allow an explicit set of local non-patchy connections to develop because only excitatory connections were explicitly modeled, and these are suppressed within the rim.

Fig. 5 shows the detail of a singularity and its surrounding pinwheel of orientation preference. This figure is taken from a simulation using a larger-scale model V1 that was stimulated with both moving bars and small blobs (the connection details are slightly different for this larger-scale experiment, see Appendix A). The diagram shows the input connectivity converging into the 64 minicolumns of the pinwheel, revealing the modulatory input map for each of the minicolumns. For minicolumns close to the pinwheel, the input map contains connections that arise only from nearby regions in the visual field. The local maps of orientation preference became self-organized such that blob-like stimuli were represented near pinwheels. In the Bosking et al. (1997) paper, tracer injection sites were chosen which had a clear orientation preference. The pattern of connections from singularities is therefore unknown.

Minicolumns not in the vicinity of the singularity show a more widespread distribution of input connections, lying along the axis of a bar-shape of appropriate orientation, and receiving inputs from the furthest reaches of the global retinotopic map. This matches the *in vivo* results of Bosking et al. (1997). The two basic patterns of connectivity, short-range connections near singularities and long-range connections away from singularities, match the hub and spoke pattern of local map connectivity assumed in the geometric model. In the neural network simulations this local map connectivity is not assumed but arises through self-organization.

The spatial tiling of orientation patches in the neural network simulations is quasi-random in nature, particularly in the larger simulations where the boundary conditions of the simulated cortex play a lesser role (data not shown). The changing spatial frequencies of orientation patches at different locations are due to the changing tiling patterns between rotated and reflected variants of the basic local map. This noisiness in the overall map of orientation preference contrasts to the clear connectivity structure that arises when inputs into individual orientation pinwheels are analyzed.

### 4.4. Discussion of modeling

The development of this local map connectivity is not critically dependent on any of the parameter settings in the simulations (see Appendix A). Instead, the critical criteria appear to be

1. The opportunity for any point in retinotopic map to potentially influence any other point.
2. The presentation of varying types of stimuli such a long bars as well as blobs.
3. Use of the coherent infomax learning rule.

Criterion one allows the possibility for the long-range connections. Criterion two requires the maps to self-organize to efficiently represent stimuli of different length or orientation. Criterion three allows each local map to gain a representation of all the contexts relevant to its own activity, rather than just the most common contexts. Together these mechanisms result in the formation of hub and spoke local map connectivity. Assumption one also appears to make the development of local maps, *which make use of inputs from the entire global retinotopic map*, inevitable and inexorable, and relatively insensitive to the other details of the simulation, making the simulations robust to parameter variation, in contrast to some other models (c.f. Swindale, 1992, 1996; see Appendix A).

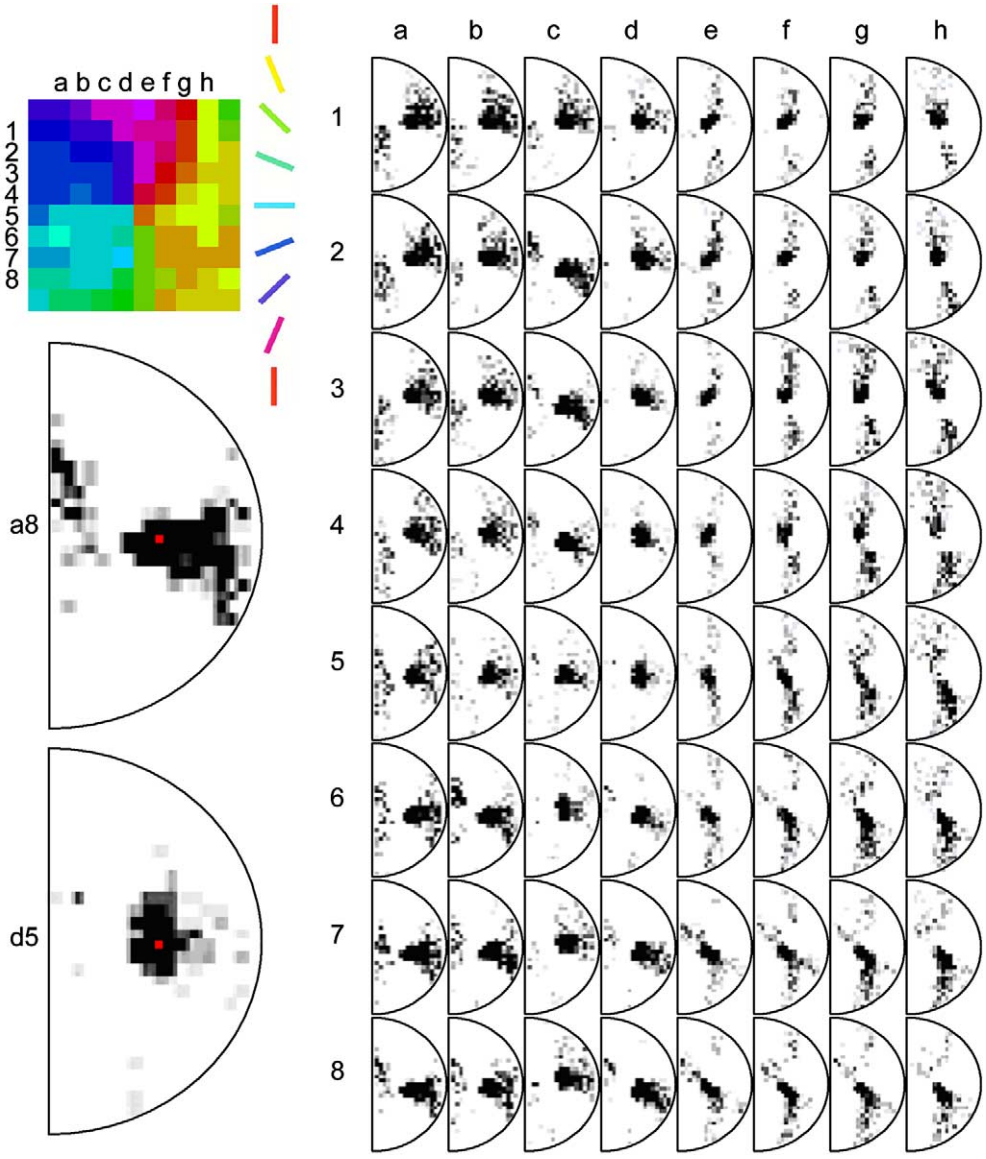


Fig. 5. Detail of local map and corresponding inputs from a simulation using type II indirect connectivity. In this simulation, the network was stimulated with bars and small blobs. Upper left of figure shows detail of a singularity and its surrounding map of orientation preference. Right of figure shows the map of indirect inputs from layer 4 to each of the 64 minicolumns in the supragranular layers. Indirect input weights vary from 0 (white) to 0.005 (black). This pinwheel was located in the middle of the global V1 map i.e. near the horizontal meridian about 25° eccentricity. In the center of the pinwheel, the indirect inputs arise from the center of V1 global map i.e. where this pinwheel is located retinotopically. At the edges of the pinwheel, inputs arise more from the furthest extent of the global map. The orientation preference of the minicolumn is defined by both the presence of strong connections overlying a line of that orientation, and by the lack of connections in along an orthogonal axis. Bottom left of figure shows the detail of input maps for two minicolums, a8 and d5. The site of the orientation pinwheel within the global map (i.e. the injection site within the input layer) is shown with a red dot.

It may be objected that real anatomical connections do not support this hypothetical one-to-all projection, even when all horizontal connections in developing V1 are considered. As we described in Section 2, the developmental trajectory of the long-range horizontal connections in the tree shrew remains unclear. Dynamic modeling considerations (Chapman et al., 2002; Robinson et al., 1998; Wright, 1997; Wright et al., 2000) and experimental findings (Gray et al., 1989; Singer & Gray, 1995) indicate that overlapping fields of synchronous oscillation could achieve a functional equivalence to the required one-to-all system of input projections. This argument was outlined in Section 3. The neural network simulation achieves directly the long-range interactions that synchrony would provide by more complex means.

It has been demonstrated that the initial phase of the development of patchy connections can occur with no

visual input (Ruthazer & Stryker, 1996). This finding suggests the formation of orientation preference is partly under the control of innate variables, as well as spontaneous cortical activity. In the neural network simulations we have assumed that horizontal connections in the tree shrew develop from visual experience of oriented lines. The arguments presented at the end of Section 3, however, suggest that visuotopically organized local maps may arise from random visual inputs. If poorly defined patchy connectivity is also found in the tree shrew prior to visual experience, this does not rule out the hypothesized connectivity structure.

Whatever the developmental mechanism, the existence of very long-range horizontal patchy connections in the mature tree shrew is not in dispute. The neural network simulations presented here are not sophisticated enough to fully match the recent data on the distribution of very long-range horizontal connections in tree shrew V1 (Chisum et al., 2003). The inclusion of realistic dynamics in simulations, of the kind described in Section 3, would likely improve the matches between both the anatomical connectivity patterns and the functional connectivity. The simulated horizontal patterns of connectivity are therefore best interpreted in functional terms. Further in vivo length summation experiments, using line stimuli subtending up to 50° visual angle, are required to establish the whether the maximum extent of functional connectivity is ~80% or ~100% of tree shrew V1.

In this section we presented evidence for a novel reinterpretation of the connectivity patterns of horizontal connections in the tree shrew. By taking the local map structure *as an assumption* in the geometric model, the larger scale patterns of connectivity that result from large injections of tracer were reproduced. In addition, we have used a neural network simulation to demonstrate that the hypothesized local map structure arises, *de novo*, through self-organization.

Since the modeling was intended to demonstrate the hub and spokes local connectivity map, we did not attempt to model all the features measurable in the map of orientation preference, such as tuning width of individual cells. We also assume that the exact tiling pattern found is determined by the exact details of development for that particular animal, in particular the spatial autocorrelation statistics of stimuli to which the animal is exposed, and that it has a quasi-random character similar to the development of magnetic spin networks. The exact densities of singularities, linear zones and saddle-points, and density ratios between these features, are not therefore considered of primary importance. Instead, we present predictions relating the presence of these features to the underlying patterns of connectivity, in vivo.

The specific predictions arising from the two types of modeling presented in this paper are as follows:

1. Singularities in the tree shrew will have shorter-range horizontal connectivity than saddle-points or linear zones. This is an a priori prediction of the LGM hypothesis, and has since been confirmed in the cat (Yousef et al., 2001) and the ferret (Lund et al., 2003).
2. A second way to test prediction (1) is to note that singularities will appear in inter-stripe regions when very large injections of tracer are applied to the surface of the tree shrew primary visual cortex.

## 5. Conclusions

The modeling suggests that orientation preference in the tree shrew arises from local maps that tile the global retinotopic mapping in the supragranular layers. We argue that these local mappings, though not involved in the retinotopic response, are nevertheless visuotopically organized.

We can use polar coordinates to describe the relationships between minicolumns within a pinwheel of orientation preference (coordinates of $(\theta, r)$ around a singularity, $p$) and locations in the global retinotopic map (coordinates of $(\Theta, R)$ around a point in the visual field, $P$). The modeling described in this paper has similar patterns of intrinsic connectivity as found in vivo in the tree shrew (Bosking et al., 1997). Minicolumns located away from the singularity (i.e. large $r$) receive inputs from of the visual field from *within* a large radius $R$, along an axis of orientation $\Theta$. We refer to these long-range connections as spokes. They help tune the response properties of the minicolumn to a corresponding orientation preference of $\theta$. In addition, the neural network simulations self-organized such that minicolumns within small radius, $r$, of a singularity receive indirect inputs from within a small radius, $R$, of the visual field. We refer to this short-range connectivity as the hub. In the geometric model, tiling patterns of local maps of hub and spoke connectivity were shown to be consistent with patterns of connectivity seen for large injections of tracer into the upper layers of tree shrew V1.

In Section 3 we outlined the mechanisms for the creation of visuotopically organized maps. The relevant criteria for visuotopically organized local maps are as follows:

1. Each local map makes use of inputs from (almost) the entire extent of V1.
2. The response properties at points in the local map vary systematically as a function of the regions of the global map from which they receive inputs.

Both these criteria are met in the case of hub and spokes local map connectivity. In addition, the mapping from the global map to the local map is not 1:1, but

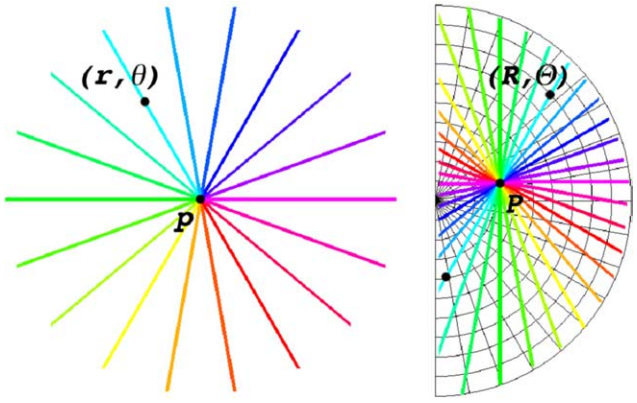


Fig. 6. Summary of idealized visuotopic mapping for inputs into pinwheels of orientation preference. Left: A minicolumn within a pinwheel can be ascribed polar coordinates ($r$, $\theta$) indicating that it is located at a radius $r$ from the singularity $p$, and with an orientation preference $\theta$. Right: Such a minicolumn will receive inputs from an extent of the visual field from *within* a radius $R$ on a line passing through $P$ with orientation of $\Theta$. The pinwheel itself is located at point $P$ in the global retinotopic space. The relationships between points in the local map (lower-case letters) and points in the global map (upper-case letters) are specified by Eq. (1) in the main text. The mapping describes the idealized case and in practice the input mapping is a noisy version of this ideal case. When expressed in terms of stimulus properties, a line of radius $R$ and orientation $\Theta$ passing through point $P$ in the global map is represented at ($r$, $\theta$) in the local map. See also in the main text for the purported relationship between this smooth mapping of orientation preference and the assumed underlying discrete, columnar connectivity structure.

eliminates some redundancies, as well as adding redundancies where parts of the global map are common to multiple representations within a local map.

The shape of each local map is therefore *approximately* visuotopic. The transformation from the hemi-retina to the local map can be expressed in an idealized form as a conformal mapping in the $z$-plane, from the global map, $Z$, to the local map, $z$. This conformal mapping is illustrated in Fig. 6 and is given by the following equation: [2]

$$z = \frac{(Z-P)^2}{|Z-P|} \tag{1}$$

Note that the distance $|Z-P|$ refers to the *maximum extent* of the global map from which the local map receives inputs. This reflects the connectivity redundancies along the radial dimension, due to commonalities in the representations of lines of various lengths. In each of the local maps, the hemi-retinal visuotopy is also distorted so that $\pi$ angles of line orientation are represented in $2\pi$ of the local map. This has the effect of eliminating redundancies in the polar dimension around $P$ that arise with elongated stimuli.

When the mapping in Eq. (1) is conceived in terms of stimulus properties, $R$ and $\Theta$ correspond to the radius and orientation of a globally represented line—which we take to be a *primitive* feature to which the tree shrew primary visual cortex responds. Defined in this way, the equation describes a simple mapping of global primitive parameters ($R$, $\Theta$) to local maps of non-retinotopic response properties $(r, \theta)$. The relationship between oriented lines and orientation preference was outlined at the end of Section 2. The mapping also implies that non-oriented small blobs ($R \cong 0$) are represented at $r \cong 0$, which also defines the property of low orientation selectivity. Length preference, for lines $R > 0$, is represented by $r$. The specific functional prediction that arises out of the LGM hypothesis for the tree shrew is that longest length preferences (40°+) will be represented away from singularities. This can be tested experimentally with a combination of optical imaging and single cell recording.

The LGM hypothesis of the primary visual cortex suggests there is a rather direct relationship between globally represented objects and various response properties that have a local geometry. The local map at retinotopic point $P$ learns about the set of stimuli, $S$, which activate $P$ i.e. pass over that point. The singularity is formed at point $p$ in the local map, where $p$ is the point in the local visuotopic map that corresponds to the point $P$ in the global retinotopic map. In other words, *the singularity is the local map representation of the position of the local map in the global retinotopic space*. This is the pattern of relationships predicted by the LGM hypothesis and can be stated succinctly as visuotopically organized local maps of non-retinopic response properties. Together the global and local visuotopically organized mappings demonstrate the LGM hypothesis of V1 (Alexander et al., 1998); for the tree shrew at least.

The LGM interpretation of the origin of response properties implies a functional consequence supplementary to that of the dimension-reduction models mentioned in the introduction. Dimension reduction implies that an efficient packing of afferent information onto the two-dimensional cortical surface has taken place. The LGM hypothesis indicates that this mapping is also such as to enable any and all local neural processing to make use of information originating from a much greater extent of the visual field than has previously been theorized. In essence, the LGM creates a four-dimensional representational space on the surface of V1. In this space, properties of the two-dimensional visual field are represented twice; once as the global retinotopic map and once as a local map of modulatory response properties.

[2] This mapping, expressed in continuous form, applies to the response properties. The discrete form of the mapping applies to the underlying columnar organization of horizontal fibers. The relationship between these two forms is discussed at the beginning of Section 4.

A key argument against the idea that V1 is organized from a fundamental repeating unit involves the observation that different response properties are not tightly interlocked across the surface of V1 (Hubener et al., 1997; Swindale et al., 2000). The observation does not rule out the LGM hypothesis, however, since the tiling of the local map is highly variable. As noted in Section 4, the tiling patterns of the local map result in different orientation patches having markedly different spatial frequencies, depending on the exact tiling pattern (saddle-points or linear zones) and overall rotation of the local map. In addition, it is a prediction of the LGM hypothesis that relationships between CO blobs and orientation preference (in the macaque) will change systematically with retinotopic location; and evidence supporting this prediction has recently been published (Vanduffel, Tootell, Schoups, & Orban, 2002). The existence of a visuotopically organized local map of non-retinotopic response properties does not imply a rigid tiling of response property systems.

As noted earlier, the learning rule applied here is derived from the coherent infomax principle (Kay & Phillips, 1997; Phillips & Singer, 1998). Coherent infomax learning maximizes the transmission of contextually related information, rather than maximizing information transmission *per se*. Our simulation results appear to provide a concrete instance of this abstract information-theoretic principle in action, since the patchy connections act to tile the visual cortex with information from the entire global retinotopic map, thereby retaining maximal contextual information. Points in the visual image can discover those visual contexts that are predictively related to their own activity. When the relevant contexts are oriented lines of various lengths, each point in the global map forms a local map of all possible lines that can pass through that point. We have argued that this local map of visual contexts involves inputs from the entire extent of V1, and is itself visuotopically organized.

Finally it may be remarked that LGM principles, generalized beyond V1, carry strong implications for the development of connectivity elsewhere in the brain.

## Acknowledgements

The research was supported by the Australian Research Council.

Thanks go to SGI for use of their 32 processor Origin series supercomputer and to George Couyant at the Melbourne SGI office. Thanks also to the Pratt group of companies for use of computing resources at the Brain Dynamics Laboratory, Mental Health Research Institute of Victoria.

## Appendix A. Details of neural network simulations

In the simulations of horizontal connectivity in the tree shrew reported here we assumed excitatory long-range intra-cortical connections based on the anatomy seen in supragranular layers in the tree shrew (called *type I* indirect inputs). Each minicolumn in the supragranular layer was potentially connected to every other minicolumn at the beginning of visual development. This first type of indirect connectivity scales as the square of the number of minicolumns, $N_m$, in the supragranular layer, limiting the size of the simulations. These size limitations meant that we were only able to present one type of stimuli, namely oriented bars. $(N_m)^2$ can be rewritten as $(N_G \times N_l)^2$ where $N_G$ is the number of global retinotopic locations and $N_l$ is the number of minicolumns within each global location.

In a second class of simulation, we used another type of long-range intra-cortical connectivity that connected each retinotopic location in the input layer to every minicolumn in the supragranular layer (called *type II* indirect inputs). The number of type II indirect connections scaled as $N_G^2 \times N_l$, enabling much larger simulations. Within these larger simulations we were able to present more varied types of stimuli (short blobs and long bars). The type II indirect connections were used instead of type I solely out of computational necessity. Even with the computational savings of type II indirect inputs, these larger simulations took over a week to run on a 32 processor SGI, and required 8 gigabytes of RAM. In the simulations these two types of indirect connectivities proved to be functionally identical, when judged by the qualitative features of the orientation maps. Type I and type II indirect connectivities are illustrated in Fig. 3.

Both model types had a set of input connections (called *direct* connections) which supplied retinotopic inputs from the granular layer to the supragranular layer. Orientation preferences were formed through an interaction of the direct inputs into the supragranular layers with the indirect inputs, when driven by visual stimuli.

A single line was presented to the simulated retina, and the line swept across, each sweep taking place at randomly chosen angles. The line was moved by one retinal pixel per presentation time-step. The presentation of a line to the retina is illustrated in Fig. 4c. In the larger experiments, small blobs (lines of length equal to their width) were also swept across the retina. The experiments with moving lines and blobs were run to see if the indirect connections would self-organise in a manner that distinguished these two types of stimuli.

The activity of each supragranular unit (corresponding to a minicolumn, 30 μm in diameter) was calculated in four steps. The symbols $a$, $b$, $c$, $d$ and $e$ denote the activations at successive stages and describe

the (a) activations on the retina, the effect of (b) direct (retinotopic) input connections, (c) indirect input connections, (d) local excitatory influence and (e) inhibitory surround, respectively and cumulatively. The activation, $a$, on the retina was fed directly to the model cortical minicolumns. No learning occurred in relation to these direct, retinotopic projections, $w_{dj}$, as they can be assumed to be largely innately provided. Eq. (2) describes the effects of the direct connections on the activation of each minicolumn:

$$b_j = w_{dj}a_d + \varepsilon, \quad a_d \in \{0,1\}, \;\; w_{dj} \in \{0,1\} \tag{2}$$

where $w_{dj}$ is the connection weight from a point in the model input layer to a point in the model supragranular layer. In the results described in this paper, the number of minicolumns at each retinotopic location in the supragranular layer was set to 100 i.e. a 10 by 10 square. Each $w_{dj}$ connected one of the $N_G$ retinotopic points in the input layer to one of the $N_l$ minicolumns directly 'above' it in the supragranular layer. An amount of white noise, $\varepsilon$, was added at this stage. The modeling results proved robust to a wide range of noise values ($0 \leqslant \varepsilon_{max} \leqslant 0.5$). The retinotopic map of the granular layer was modeled after the tree shrew, and approximated as a semi-circle.

The indirect connections, $w_{ij}$, were initially set to low values drawn from a uniform random distribution. Eq. (3a) shows the contribution to activations from indirect connections in the case where type I were used:

$$c_j = b_j + \sum_{i=1}^{N_m} w_{ij}b_i, \quad b_i \in [0,1],$$
$$\sum_{i=1}^{N_m} w_{ij} = 0.5, \;\; w_{ij} \geqslant 0 \tag{3a}$$

Eq. (3b) shows the contribution of indirect connections in the case where type II were used:

$$c_j = b_j + \sum_{i=1}^{N_G} w_{ij}a_i, \quad a_i \in \{0,1\},$$
$$\sum_{i=1}^{N_G} w_{ij} = 0.5, \;\; w_{ij} \geqslant 0 \tag{3b}$$

The excitatory-center and inhibitory-surrounds were not modeled explicitly as local patterns of connection, for reasons of computational efficiency. The excitatory-center was implemented by simply averaging the activities of each cell with its immediate neighbors:

$$d_j = \frac{\sum_{i=1}^{N_H} c_i}{N_H} \tag{4}$$

where $N_H$ is the number of minicolumns within the Mexican-hat radius. In the present modeling the Mexican-hat radius was set to 7 minicolumns. Eq. (4) has the effect of locally smoothing the activations.

The inhibitory-surround was implemented in the following fashion: the number of minicolumns, within the Mexican-hat radius, with activity lower than the $j$th cell was divided by the total number of columns within the Mexican-hat radius. The resulting quotient was then multiplied by the activity of the minicolumn with the highest activation within the Mexican-hat radius.

$$e_j = d_{H\,max}\frac{N_{low}}{N_H} \tag{5}$$

where $N_{low}$ is the number of minicolumns within the Mexican-hat radius that satisfy the condition $d_j > d_H$. $d_{H\,max}$ is the activation of the minicolumn which had the highest activation within that $d_j$'s Mexican-hat radius. Eq. (5) essentially implements a soft winner-takes-all rule. A number of different methods for calculating the Mexican-hat field were trialed and this method was found to be satisfactory but computationally simple. Varying the Mexican-hat radius had the effect of changing the spatial frequency of the singularities in the orientation preference map. An important factor to note is that the simulation results did not depend on a strict relationship between $N_l$—the size of the thalamic input 'blocks', and $N_H$—the number of minicolumns within the Mexican-hat radius.

The learning rule was a variant of Hebbian learning, an approximation of the learning rule described by Phillips and Singer (1998). The indirect connections were strengthened only when a minicolumn was active due to the direct, retinotopic projections. The learning rules for the two types of indirect connections are given in Eqs. (6a) and (6b) for type I and type II, respectively.

$$\Delta w_{ij} = ge_i(e_j - \bar{e}_j(t))|e_j - \bar{e}_j(t)|, \quad e_i \in [0,1] \tag{6a}$$

$$\Delta w_{ij} = ga_i(e_j - \bar{e}_j(t))|e_j - \bar{e}_j(t)|, \quad a_i \in \{0,1\} \tag{6b}$$

were $g$ was a constant affecting the learning rate. $g$ could be varied over a broad range of values ($3 \times 10^{-6} \leqslant g \leqslant 1 \times 10^{-4}$) without any substantive effect on the modeling results. $\bar{e}_j(t)$ was a rolling average for the $j$th minicolumn at time $t$, approximated by

$$\bar{e}_j(t) = \bar{e}_j(t-1) + \frac{e_j - \bar{e}_j(t-1)}{n_{av}} \tag{7}$$

where $n_{av}$ is the number of time steps over which the rolling average was calculated. In the present results $n_{av}$ was set to 50. Again, this parameter could be varied over a large range (20–1000) without affecting the substantive results.

The sum of the indirect weights to a given minicolumn was periodically scaled to a constant during the simulation (see Eqs. (3a) and (3b)). This was assumed to reflect some optimal metabolic load for the number of synapses on each neuron. Without this regular scaling, the magnitudes of activity were less even, but the maps of orientation preference were qualitatively

indistinguishable from the runs that included the weight normalization.

The orientation preference map was produced in a manner similar to studies in vivo. During the data collection phase, a series of 16 oriented lines of angle $\Theta$ were swept across the model retina, and the resultant activations in each minicolumn represented as vectors, $\underset{\rightarrow}{M}_{\Theta,j}$. The orientation of this vector, $\Theta$, is the orientation of the bar and the magnitude of the vector is the activation of the $j$th minicolumn in response to that bar, $e_j$.

$$\underset{\rightarrow}{M}_{\Theta,j} = (\Theta, e_j) \tag{8}$$

The orientation preference of the $j$th minicolumn, $\theta_j$, is the orientation of the vector sum of $\underset{\rightarrow}{M}_{\Theta,j}$'s measured for 16 stimulus bars. The orientation selectivity of the $j$th minicolumn, $m_j$, is the magnitude of the vector sum.

$$(\theta_j, m_j) = \sum_{\Theta=\pi/8}^{2\pi} \underset{\rightarrow}{M}_{\Theta,j}, \quad \Theta \in [\pi/8, \pi/4, \ldots, 2\pi] \tag{9}$$

The experimental variations trialed included: altering the learning and noise parameters and several types of the Hebbian learning. Each parameter could be varied individually by an order of magnitude without affecting the results, with the exception of the Mexican-hat radius, which could be varied between 6 and 12 minicolumns without affecting the 'well-formedness' of the maps of orientation preference. The robustness of the results is also indicated by the similarity of the orientation preference maps when type I or type II indirect inputs were used. The results suggest the two types of indirect connections are functionally the same.

## References


Alexander, D. M., Bourke, P. D., Sheridan, P., Konstandatos, O., & Wright, J. J. (1998). Emergent symmetry of local and global maps in the primary visual cortex: Self-organization of orientation preference. *Proceedings, Complex Systems 98*, pp. 25–31.

Angelucci, A., Levitt, J. B., Walton, E. J., Hupe, J. M., Bullier, J., & Lund, J. S. (2002). Circuits for local and global signal integration in primary visual cortex. *Journal of Neuroscience, 22*(19), 8633–8646.

Angelucci, A., & Bullier, J. (in press). Reaching beyond the classical receptive field of V1 neurons: Horizontal or feedback axons? *The Journal of Physiology (Paris)*.

Basole, A., White, L. E., & Fitzpatrick, D. (2003). Mapping multiple features in the population response of visual cortex. *Nature, 423*, 986–990.

Blasdel, G. G., & Fitzpatrick, D. (1984). Physiological organization of layer 4 in macaque striate cortex. *Journal of Neuroscience, 4*(3), 880–895.

Blasdel, G. G., Lund, J. S., & Fitzpatrick, D. (1985). Intrinsic connections of macaque striate cortex: Axonal projections of cells outside lamina 4c. *Journal of Neuroscience, 5*(12), 3350–3369.

Blasdel, G. G., & Salama, G. (1986). Voltage-sensitive dyes reveal a modular organization in monkey striate cortex. *Nature, 321*, 579–585.

Blasdel, G. G. (1992). Orientation selectivity, preference, and continuity in monkey striate cortex. *Journal of Neuroscience, 12*(8), 3139–3161.

Bosking, W., & Fitzpatrick, D. (1995). Physiological correlates of anisotropy in horizontal connections: Length summation properties of neurons in layers 2 and 3 of tree shrew striate cortex. *Society of Neuroscience Abstract, 21*, 1751.

Bosking, W. H., Crowley, J. C., & Fitzpatrick, D. (2002). Spatial coding of position and orientation in primary visual cortex. *Nature Neuroscience, 5*(9), 874–882.

Bosking, W. H., Zhang, Y., Schofield, B., & Fitzpatrick, D. (1997). Orientation selectivity and the arrangement of horizontal connections in tree shrew striate cortex. *Journal of Neuroscience, 17*(6), 2112–2127.

Braitenberg, V., & Schuz, A. (1991). *Anatomy of the cortex: Statistics and geometry*. Berlin: Springer.

Bringuier, V., Chavane, F., Glaeser, L., & Frégnac, Y. (1999). Horizontal propagation of visual activity in the synaptic integration field of area 17 neurons. *Science, 283*, 695–699.

Chapman, C. L., Bourke, P. D., & Wright, J. J. (2002). Spatial eigenmodes and synchronous oscillation: Coincidence detection in simulated cerebral cortex. *Journal of Mathematical Biology, 45*, 57–78.

Chisum, H. J., Mooser, F., & Fitzpatrick, D. (2003). Emergent properties of layer 2/3 neurons reflect the collinear arrangement of horizontal connections in tree shrew visual cortex. *Journal of Neuroscience, 23*(7), 2947–2960.

Constantine-Paton, M., Cline, H. T., & Debski, E. (1990). Patterned activity, synaptic convergence, and the NMDA receptor in developing visual pathways. *Annual Review of Neuroscience, 13*, 128–129.

Crowley, J. C., Bosking, W. H., Foster, M., & Fitzpatrick, D. (1996). Development of horizontal connections in layer 2/3 of tree shrew striate cortex: Relation to maps of orientation preference. *Neuroscience Abstract, 22*, 1016.

Durbin, R., & Mitchison, G. (1990). A dimension reduction framework for understanding cortical maps. *Nature, 343*, 644–647.

Durbin, R., & Willshaw, D. J. (1987). An analogue approach to the travelling salesman problem using an elastic net method. *Nature, 326*, 689–691.

Eckhorn, R., Bruns, A., Saam, M., Gail, A., Gabriel, A., & Brinksmeyer, H. J. (2001). Flexible cortical gamma-band correlations suggest neural principles of visual processing. *Visual Cognition, 8*(3/4/5), 519–530.

Edwards, D. P., Purpura, K. P., & Kaplan, E. (1995). Contrast sensitivity and spatial frequency response of primate cortical neurons in and around the cytochrome oxidase blobs. *Vision Research, 35*(11), 1501–1523.

Fitzpatrick, D. (1996). The functional organization of local circuits in visual cortex: Insights from the study of tree shrew striate cortex. *Cerebral Cortex, 6*(3), 329–341.

Freeman, W. J., & Barrie, J. M. (2000). Analysis of spatial patterns of phase in neocortical gamma EEGs in rabbit. *Journal of Neurophysiology, 84*(3), 1266–1278.

Friedlander, M. J., Fregnac, Y., & Burke, J. P. (1993). Temporal covariance of postsynaptic membrane potential and synaptic input—role in synaptic efficacy in the visual cortex. *Progress in Brain Research, 95*, 207–223.

Frien, A., & Eckhorn, R. (2000). Functional coupling shows stronger stimulus dependency for fast oscillations than for low-frequency components in striate cortex of awake monkey. *European Journal of Neuroscience, 12*(4), 1466–1478.

Goodhill, G. J. (1993). Topography and ocular dominance: A model exploring positive correlations. *Biological Cybernetics, 69*, 109–118.

Gray, C. M., Engel, A. K., Konig, P., & Singer, W. (1992). Synchronization of oscillatory neuronal responses in cat striate cortex: Temporal properties. *Visual Neuroscience, 8*, 337–347.

Gray, C. M., Konig, P., Engel, A. K., & Singer, W. (1989). Oscillatory responses in cat visual cortex exhibit intercolumnar synchronisation which reflects global stimulus properties. *Nature, 388*, 334–337.

Grinvald, A., Lieke, E. E., Frostig, R. D., & Hildesheim, R. (1994). Cortical point-spread function and long-range lateral interactions revealed by real-time optical imaging of macaque monkey primary visual cortex. *Journal of Neuroscience, 14*, 2545–2568.

Horton, J. C., & Hubel, D. H. (1981). Regular patchy distribution of cytochrome oxidase staining in primary visual cortex of macaque monkey. *Nature, 292*(5825), 762–764.

Hubel, D. H., & Wiesel, T. N. (1968). Receptive fields and functional architecture of the monkey striate cortex. *Journal of Physiology (London), 195*, 215–243.

Hubel, D. H., & Wiesel, T. N. (1977). Functional architecture of macaque monkey visual cortex. *Proceedings of the Royal Society (B), 198*, 1–59.

Hubener, M., Shoham, D., Grinvald, A., & Bonhoeffer, T. (1997). Spatial relationships among three columnar systems in cat area 17. *Journal of Neuroscience, 17*(23), 9270–9284.

Kay, J., & Phillips, W. A. (1997). Activation functions, computational goals and learning rules for local processors with contextual guidance. *Neural Computation, 9*, 763–768.

Kohonen, T. (1982). Self-organized formation of topologically correct feature maps. *Biological Cybernetics, 43*, 59–69.

Lee, T. S. (2002). Top-down influence in early visual processing: A Bayesian perspective. *Physiology and Behavior, 77*, 645–650.

Linsker, R. (1986). From basic network principles to neural architecture: emergence of orientation columns. *Proceedings of the National Academy of Sciences USA, 83*, 8779–8783.

Livingstone, M. S. (1996). Oscillatory firing and interneuronal correlations in squirrel monkey striate cortex. *Journal of Neurophysiology, 75*(6), 2467–2485.

Lund, J. S., Angelucci, A., & Bressloff, P. C. (2003). Anatomical substrates for functional columns in macaque monkey primary visual cortex. *Cerebral Cortex, 13*(1), 15–24.

Lyon, D. C., Jain, N., & Kaas, J. H. (1998). Cortical connections of striate and extrastriate visual areas in tree shrews. *Journal of Comparative Neurology, 401*(1), 109–128.

Malach, R., Amir, Y., Harel, M., & Grinvald, A. (1993). Relationship between intrinsic connections and functional architecture revealed by optical imaging and in vivo targeted biocytin injections in primate striate cortex. *Proceedings of the National Academy of Sciences of the United States of America, 90*(22), 10469–10473.

Miller, K. D., Keller, J. B., & Stryker, M. P. (1989). Ocular dominance column development: Analysis and simulation. *Science, 245*, 605–615.

Mitchison, G., & Crick, F. (1982). Long axons within the striate cortex: their distribution, orientation, and patterns of connection. *Proceedings of the National Academy of Sciences of the United States of America, 79*(11), 3661–3665.

Mitchison, G., & Durbin, R. (1986). Optimal numberings of an $N \times N$ array. *SIAM Journal of Algebraic and Discrete Methods, 7*, 571–578.

Obermayer, K., Ritter, H., & Schulten, K. (1990). A principle for the formation of the spatial structure of cortical feature maps. *Proceedings of the National Academy of Sciences USA, 87*, 8345–8349.

Phillips, W. A., & Singer, W. (1998). In search of common foundations for cortical computation. *Behavioral and Brain Sciences, 20*, 657–722.

Rauschecker, J. P. (1990). Mechanisms of visual plasticity: Hebb synapses, NMDA receptors, and beyond. *Physiological Review, 71*, 587–615.

Rennie, C. J., Wright, J. J., & Robinson, P. A. (2000). Mechanisms of cortical electrical activity and the emergence of gamma rhythm. *Journal of Theoretical Biology, 205*, 17–35.

Robinson, P. A., Wright, J. J., & Rennie, C. J. (1998). Synchronous oscillations in the cerebral cortex. *Physical Review E, 57*, 4578–4588.

Rockland, K. S., & Lund, J. S. (1982). Widespread periodic intrinsic connections in the tree shrew visual cortex. *Science, 215*(4539), 1532–1534.

Rockland, K. S., & Lund, J. S. (1983). Intrinsic laminar lattice connections in primate visual cortex. *Journal of Comparative Neurology, 216*, 303–318.

Rockland, K. S., & Knutson, T. (2001). Axon collaterals of meynert cells diverge over large portions of area V1 in the Macaque Monkey. *The Journal of Comparative Neurology, 441*, 134–147.

Ruthazer, E. S., & Stryker, M. P. (1996). The role of activity in the development of long-range horizontal connections in area 17 of the ferret. *Journal of Neuroscience, 16*(22), 7253–7769.

Schwartz, E. L. (1980). Computational anatomy and functional architecture of striate cortex: A spatial mapping approach to perceptual coding. *Vision Research, 20*, 645–669.

Singer, W., & Gray, C. M. (1995). Visual feature integration and the temporal correlation hypothesis. *Annual Review of Neuroscience, 18*, 555–586.

Slovin, H., Arieli, A., Hildesheim, R., & Grinvald, A. (2002). Long-term voltage-sensitive dye imaging reveals cortical dynamics in behaving monkeys. *Journal of Neurophysioly, 88*, 3421–3438.

Swindale, N. V. (1992). A model for the coordinated development of columnar systems in primate striate cortex. *Biological Cybernetics, 66*, 217–230.

Swindale, N. V. (1996). The development of topography in the visual cortex: A review of models. *Network, 7*, 161–247.

Swindale, N. V., Shoham, D., Grinvald, A., Bonhoeffer, T., & Hubener, M. (2000). Visual cortex maps are optimized for uniform coverage. *Nature Neuroscience, 3*(8), 822–826.

Tanaka, S. (1989). Theory of self-organization of cortical maps. In D. S. Touretzky (Ed.), *Advances in neural information processing systems I* (pp. 451–458). San Mateo: Morgan Kauffman.

Tootell, B. H., Switkes, E., Silverman, M. S., & Hamilton, S. L. (1988). Functional anatomy of the macaque striate cortex. II. Retinotopic organization. *Journal of Neuroscience, 8*(5), 1531–1568.

Tootell, B. H., Silverman, M. S., Hamilton, S. L., Switkes, E., & De Valois, R. (1988). Functional anatomy of the macaque striate cortex. V. Spatial frequency. *Journal of Neuroscience, 8*(5), 1610–1624.

Tootell, B. H., Silverman, M. S., Hamilton, S. L., De Valois, R., & Switkes, E. (1988). Functional anatomy of the macaque striate cortex. III. Color. *Journal of Neuroscience, 8*(5), 1569–1593.

Ungersbock, A., Kretz, R., & Rager, G. (1991). Synaptogenesis in the primary visual cortex of the tree shrew (Tupaia belangeri). *Journal of Comparative Neurology, 308*(3), 491–504.

Vanduffel, W., Tootell, R. B. H., Schoups, A. A., & Orban, G. A. (2002). The organization of orientation selectivity throughout the Macaque visual cortex. *Cerebral Cortex, 12*, 647–662.

von der Marlsburg, C. (1973). Self-organization of orientation selective cells in the striate cortex. *Kybernetic, 14*, 85–100.

Wright, J. J., Robinson, P. A., Rennie, C. J., Gordon, E., Bourke, P. D., Chapman, C. L., Hawthorn, N., Lees, G. J., & Alexander, D. M. (2001). Toward an integrated continuum model of cerebral dynamics: The cerebral rhythms, synchronous oscillation and cortical stability. *Biosystems, 63*, 71–88.

Wright, J. J. (1997). EEG simulation: Variation of spectral envelope, pulse synchrony and approx. 40Hz oscillation. *Biological Cybernetics, 76*, 181–194.

Wright, J. J., Bourke, P. D., & Chapman, C. L. (2000). Synchronous oscillation in the cerebral cortex and object coherence: Simulation of basic electrophysiological findings. *Biological Cybernetics, 83*, 341–353.

Yoshioka, T., Blasdel, G. G., Levitt, J. B., & Lund, J. S. (1996). Relation between patterns of intrinsic lateral connectivity, ocular dominance, and cytochrome oxidase-reactive regions in macaque monkey striate cortex. *Cerebral Cortex, 6*(2), 297–310.

Yousef, T., Toth, E., Rausch, M., Eysel, U. T., & Kisvarday, Z. F. (2001). Topography of orientation center connections in the primary visual cortex of the cat. *Neuroreport, 12*, 1693–1699.

Zuffery, P. D., Jin, F., Nakamura, H., Tettoni, L., & Innocenti, G. M. (1999). The role of pattern vision in the development of cortico-cortical connections. *European Journal of Neuroscience, 11*, 2669–2688.